# JOURNAL
## OF THE
# AMERICAN CHEMICAL SOCIETY

# Characterization of a Substrate-Derived Radical Detected during the Inactivation of Ribonucleotide Reductase from *Escherichia coli* by 2′-Fluoromethylene-2′-deoxycytidine 5′-Diphosphate

**Gary J. Gerfen,**[†,‡,§] **Wilfred A. van der Donk,**[†,‖] **Guixue Yu,**[†,⊥] **James R. McCarthy,**[⊗,◇] **Esa T. Jarvi,**[◇] **Donald P. Matthews,**[◇] **Christian Farrar,**[†,‡] **Robert G. Griffin,**[*,†,‡] **and JoAnne Stubbe**[*,†,¶]

*Contribution from the Departments of Chemistry and Biology and the Francis Bitter Magnet Laboratory, Massachusetts Institute of Technology, Cambridge, Massachusetts 02139, and Marion Merrell Dow Research Institute, 2110 East Galbraith Road, Cincinnati, Ohio 45215*

*Received June 30, 1997*

**Abstract:** Ribonucleotide reductase (RDPR) from *E. coli* catalyzes the conversion of nucleotides to deoxynucleotides and contains an unusual tyrosyl radical−diferric cluster cofactor. (*E*)-2′-Fluoromethylene-2′-deoxycytidine 5′-diphosphate [(*E*)-**1**] obtained by phosphorylation of the clinically promising antitumor agent MDL 101,731, is a potent time-dependent inactivator of this protein. Electron paramagnetic resonance (EPR) spectroscopy reveals that inactivation is accompanied by loss of the essential tyrosyl radical cofactor and formation of a new radical species. The 9.4-GHz EPR spectrum of this new radical reveals two hyperfine splittings of approximately 1.5 mT producing a triplet-like signal. Incubation of the enzyme with [6′-²H]-(*E*)-**1** alters this EPR spectrum, providing the first evidence for a nucleotide-based radical species generated by RDPR. The observed spectrum is a 1:1 composite of a doublet and a triplet signal, the latter being identical to that obtained with unlabeled (*E*)-**1**. Studies with (*E*)-**1** in ²H₂O also produce a 1:1 mixture of these two radical signals. The results of these isotope labeling experiments suggest wash-out or wash-in of ∼0.5 equiv of deuterium at the 6′ position, respectively. Incubation of the enzyme with [6′-²H]-(*E*)-**1** in ²H₂O produced only the doublet as would be expected on the basis of this hypothesis. EPR (139.5 GHz) spectra established the principal *g* values of the new radical species. Simulation of the 9.4- and 139.5-GHz EPR spectra yield a self-consistent set of principal hyperfine values. A structure is proposed for the radical intermediate that is consistent with the EPR data and kinetic data on release of the fluoride ion that accompanies inactivation. The proposed structure and a postulated mechanism for its formation provide further support for the hypothesis that catalysis is initiated by 3′-hydrogen atom abstraction from the nucleotide substrate.

## Introduction

Ribonucleotide reductases (RNRs)[○] catalyze the rate-determining step in DNA biosynthesis, conversion of nucleotides into the corresponding deoxynucleotides.[1−4] Because of the central role in DNA metabolism, this class of enzymes has

† Department of Chemistry, Massachusetts Institute of Technology.

‡ Francis Bitter Magnet Laboratory, Massachusetts Institute of Technology.

§ Present address Department of Physiology and Biophysics, Albert Einstein College of Medicine of Yeshiva University, 1300 Morris Park Avenue, Bronx, NY 10461.

‖ Present address Department of Chemistry, University of Illinois at Urbana-Champaign, Urbana, IL 61801.

⊥ Present address Cubist Pharmaceuticals, 24 Emily Street, Cambridge, MA 02139.

⊗ Present address Neurocrine Biosciences, 3050 Science Park Road, San Diego, CA 92121.

◇ Marion Merrell Dow Research Institute.

¶ Department of Biology, Massachusetts Institute of Technology.

attracted much attention as potential targets for therapeutic antitumor and antiviral agents.[4−7] Several different strategies for inactivation of RNRs have been reported, including the use of substrate analogues as mechanism-based inhibitors.[1,4−6,8,9] Recent in vivo studies with the nucleoside analogue (E)-2′-fluoromethylene-2′-deoxycytidine (MDL 101,731) have demonstrated potent antiproliferative activity of this compound against a wide variety of tumor cell lines,[10,11] as well as humanxenografts in mice.[12,13] Its cytotoxicity has been proposed to result from the synergistic inactivation of several cellular targets that are essential for nucleic acid metabolism. The 5′-triphosphate functions as a DNA chain terminator in the DNA polymerase catalyzed elongation reaction.[10] In addition, the 5′-diphosphate, (E)-2′-fluoromethylene-2′-deoxycytidine 5′-diphosphate [(E)-**1**], rapidly and completely inactivates RNR.[10,11,14,15] Results of continuing studies on the mechanism of inactivation of RNR by this inhibitor and its geometric isomer (Z)-**1** are presented here, which provide the first direct support for 3′-hydrogen atom abstraction and the first observation of a nucleotide-based radical intermediate.



MDL 101,731    (E)-1    (Z)-1
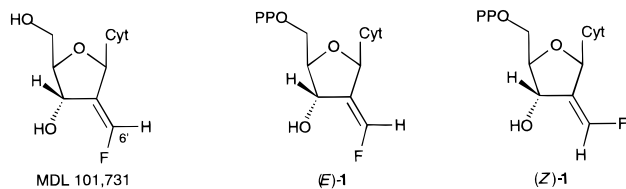
The *E. coli* ribonucleoside diphosphate reductase (RDPR) is composed of two homodimeric subunits R1 and R2 and serves as the prototype of the mammalian enzyme. R1 contains the

(1) Stubbe, J. *Adv. Enzymol. Relat. Areas Mol. Biol.* **1990**, *63*, 349−417.

(2) Reichard, P. *Science* **1993**, *260*, 1773−1777.

(3) Sjöberg, B.-M. In *Structure of Ribonucleotide Reductase from Escherichia coli*; Eckstein, F., Lilley, D. M. J., Eds.; Springer: Berlin, 1995; pp 192−221.

(4) Stubbe, J.; van der Donk, W. A. *Chem. Biol.* **1995**, *2*, 793−801.

(5) Cory, J. G.; Chiba, P. In *Combination Chemotherapy Directed at the Components of Nucleoside Diphosphate Reductase*; Cory, J. G., Cory, A. H., Eds.; Pergamon Press: New York, 1989; pp 245−264.

(6) Robins, M. J.; Samano, M. C.; Samano, V. *Nucleosides Nucleotides* **1995**, *14*, 485−493.

(7) Nocentini, G. *Crit. Rev. Oncol. Hematol.* **1996**, *22*, 89−126.

(8) Thelander, L.; Larsson, B.; Hobbs, J.; Eckstein, F. *J. Biol. Chem.* **1976**, *251*, 1398−1405.

(9) Sjöberg, B.-M.; Gräslund, A.; Eckstein, F. *J. Biol. Chem.* **1983**, *258*, 8060−8067.

(10) McCarthy, J. R.; Sunkara, P. S. In *Design, Synthesis and Antitumor Activity of an Inhibitor of Ribonucleotide Reductase*; Weiner, D. B., Williams, W. B., Eds.; CRC Press: Boca Raton, FL, 1995; pp 3−32.

(11) McCarthy, J.; Sunkara, P. S.; Matthews, D. P.; Bitonti, A. J.; Jarvi, E. T.; Sabol, J. S.; Resvick, R. J.; Huber, E. W.; van der Donk, W. A.; Yu, G.; Stubbe, J. *ACS Symp. Ser.* **1996**, *639*, 246−264.

(12) Bitonti, A. J.; Dumont, J. A.; Bush, T. L.; Cashman, E. A.; Cross-Doersen, D. E.; Wright, P. S.; Matthews, D. P.; McCarthy, J. R.; Kaplan, D. A. *Cancer Res.* **1994**, *54*, 1485−1490.

(13) Bitonti, A. J.; Bush, T. I.; Lewis, M. T.; Sunkara, P. S. *Anticancer Res.* **1995**, *15*, 1179−1182.

(14) Sunkara, P. S.; Lippert, B. J.; Snyder, R. D.; Jarvi, E. T.; Farr, R. A. *Proc. Am. Assoc. Cancer Res.* **1988**, *29*, 324.

(15) van der Donk, W. A.; Yu, G.; Silva, D. J.; Stubbe, J.; McCarthy, J. R.; Jarvi, E. T.; Matthews, D. P.; Resvick, R. J.; Wagner, E. *Biochemistry* **1996**, *35*, 8381−8391.

**Scheme 1**
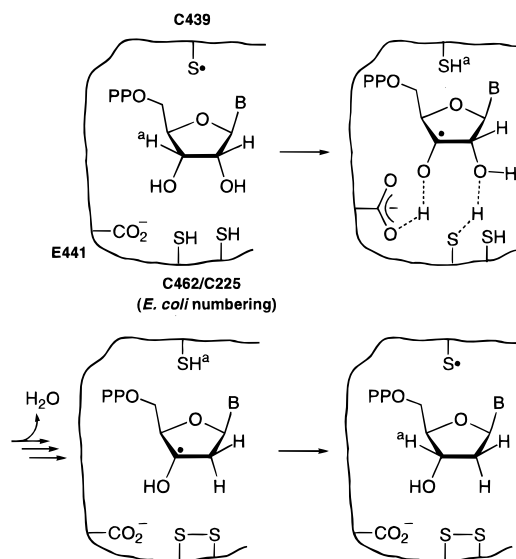


active site for reduction of both purine and pyrimidine substrates and five cysteines that are required for catalysis.[16−19] R2 contains the essential tyrosyl radical ($Y_{122}$•)−diferric cluster cofactor which is thought to generate a thiyl radical at cysteine 439 in the active site on R1 by a series of coupled electron and proton transfers.[16,20,21] As depicted in Scheme 1, this thiyl radical has been proposed to initiate catalysis by hydrogen atom abstraction from the 3′ position of the nucleotide substrate.[22] The putative substrate radical generated then loses water and is reduced with concomitant oxidation of two cysteines, Cys225-R1 and Cys462-R1, in the active site of the enzyme.[4,16] The thiyl radical on Cys439 is then regenerated by hydrogen atom transfer to the 3′-deoxyribonucleotide radical providing the reduction product. Subsequent turnovers can be achieved using either an enzymatic reduction system consisting of thioredoxin (TR), thioredoxin reductase (TRR), and NADPH or small molecular weight thiols such as dithiothreitol (DTT).

Recent EPR studies on the interaction of nucleotide substrates with the adenosylcobalamin-dependent reductase from *L. leichmannii*[23,24] and on the reaction of two mechanism-based inhibitors with *E. coli* RDPR have provided support for thiyl radical mediated chemistry.[25,26] In contrast, despite considerable effort using a variety of nucleotides,[8,9,25,27−36] direct detection

(16) Mao, S. S.; Holler, T. P.; Yu, G. X.; Bollinger, J. M.; Booker, S.; Johnston, M. I.; Stubbe, J. *Biochemistry* **1992**, *31*, 9733−9743.

(17) Thelander, L. *J. Biol. Chem.* **1974**, *249*, 4858−4862.

(18) Lin, A. I.; Ashley, G. W.; Stubbe, J. *Biochemistry* **1987**, *26*, 6905−6909.

(19) Åberg, A.; Hahne, S.; Karlsson, M.; Larrson, Å.; Ormö, M.; Åhgren, A.; Sjöberg, B. M. *J. Biol. Chem.* **1989**, *264*, 2249−2252.

(20) Stubbe, J. *J. Biol. Chem.* **1990**, *265*, 5329−5332.

(21) Uhlin, U.; Eklund, H. *Nature* **1994**, *370*, 533−539.

(22) Mao, S. S.; Yu, G. X.; Chalfoun, D.; Stubbe, J. *Biochemistry* **1992**, *31*, 9752−9759.

(23) Licht, S. L.; Gerfen, G. J.; Stubbe, J. *Science* **1996**, *271*, 477−481.

(24) Gerfen, G. J.; Licht, S. L.; Willems, J.-P.; Hoffman, B. M.; Stubbe, J. *J. Am. Chem. Soc.* **1996**, *118*, 8192−8197.

(25) van der Donk, W. A.; Stubbe, J.; Gerfen, G. J.; Bellew, B. F.; Griffin, R. G. *J. Am. Chem. Soc.* **1995**, *117*, 8908−8916.

(26) Covès, J.; Le Hir de Fallois, L.; Le Pape, L.; Décout, J.-L.; Fontecave, M. *Biochemistry* **1996**, *35*, 8595−8602.
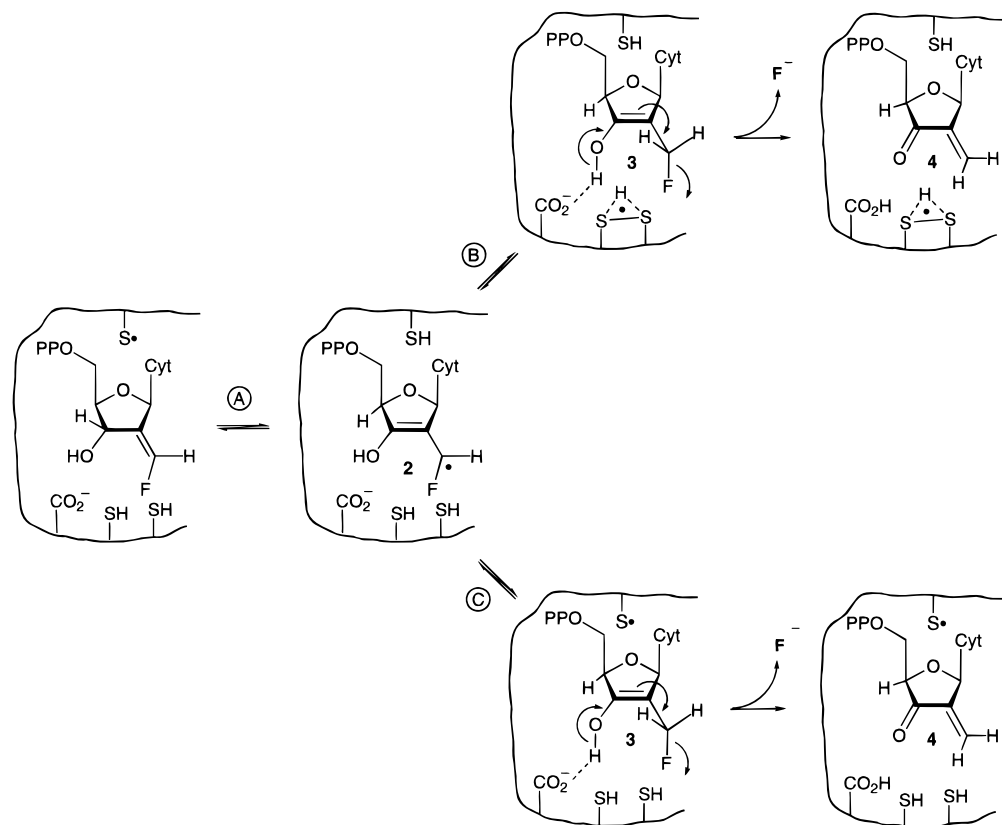
(27) Stubbe, J.; Kozarich, J. W. *J. Biol. Chem.* **1980**, *255*, 5511−5513.

(28) Stubbe, J.; Kozarich, J. W. *J. Am. Chem. Soc.* **1980**, *102*, 2505−2507.

(29) Stubbe, J.; Smith, G.; Blakley, R. L. *J. Biol. Chem.* **1983**, *258*, 1619−1624.

(30) Ator, M.; Salowe, S. P.; Stubbe, J.; Emptage, M. H.; Robins, M. J. *J. Am. Chem. Soc.* **1984**, *106*, 1886−1887.

**Scheme 2**

of *nucleotide-based radical intermediates* during catalysis has remained elusive.

The results of previous studies[15] on the inactivation of RDPR by $[6'-^{14}C]$-(*E*)-**1** established that 1.5 equiv of inhibitor is sufficient to completely abolish enzyme activity and that 1.5 equiv of fluoride and 0.5 equiv of cytosine are released during this process. Inactivation results from reduction of the tyrosyl radical on R2 and stoichiometric covalent alkylation of R1 (0.92 equiv/R1). Active-site-directed mutagenesis suggested that Glu441 is the site of labeling. Since the inactivation is thought to be initiated by the Cys439 thiyl radical, it is not surprising that covalent modification of C439S-R1 by **1** was not detected. Hence this residue cannot be ruled out as the site of labeling. Finally, a new radical species of unknown origin was detected by EPR spectroscopy during the inactivation process.

The results described above allowed us to formulate a working hypothesis for the mechanism of inactivation of RDPR by (*E*)-**1** as illustrated in Scheme 2. This model is based in part on the general paradigm that has been developed for the mechanism of inactivation of RDPR by 2′-substituted nucleotide analogues.[4,15] Hydrogen atom abstraction from the 3′ position of (*E*)-**1** would generate the fluorinated allyl radical **2** (Scheme 2). Subsequent hydrogen atom transfer from either Cys225 or Cys462 to C6′ would generate a thiyl radical which could combine with its thiol neighbor to produce a protonated disulfide

radical (pathway B).[37–39] Alternatively, hydrogen atom transfer could occur from Cys439 (pathway C). In either case, the enol intermediate **3** would be generated and rapidly lose fluoride to give **4**. The resulting $\alpha,\beta$-unsaturated ketone is highly activated toward nucleophilic addition. Such an attack by a protein residue would account for the observed R1 inactivation and the stoichiometric covalent modification of the enzyme.[15]

On the basis of the model described above, the fluorinated allyl radical **2** appeared an attractive candidate for the observed radical intermediate. Therefore, a detailed characterization of this species was undertaken using multifrequency EPR techniques and isotopic labeling of the inhibitor. These studies have established that the radical is substrate-based and permit us to propose a molecular structure and a mechanism for its generation that incorporates and extends the model depicted in Scheme 2.

## Results

**Formation and Quantitation of a New Radical in the Reaction of RDPR with (*E/Z*)-1.** Previous studies have established that inactivation of RDPR by (*E*)- or (*Z*)-**1** is accompanied by reduction of the essential tyrosyl radical on R2 and the concomitant generation of a new paramagnetic species.[15] Figure 1 shows typical 9.4-GHz EPR spectra of samples that were frozen in liquid N$_2$ 60 s after addition of 4 equiv of (*E*)-**1** or (*Z*)-**1** to the enzyme (Figure 1, parts A and D, respectively). These spectra can be explained as a superposition of two signals, one arising from residual $Y_{122}^{\bullet}$ and a second from a new radical species.[15] Attempts to eliminate the $Y^{\bullet}$

(31) Harris, G.; Ator, M.; Stubbe, J. *Biochemistry* **1984**, *23*, 5214–5225.

(32) Ator, M. A.; Stubbe, J. *Biochemistry* **1985**, *24*, 7214–7221.

(33) Salowe, S. P.; Ator, M.; Stubbe, J. *Biochemistry* **1987**, *26*, 3408–3416.

(34) Harris, G.; Ashley, G. W.; Robins, M. J.; Tolman, R. L.; Stubbe, J. *Biochemistry* **1987**, *26*, 1895–1902.

(35) Ashley, G. W.; Harris, G.; Stubbe, J. *Biochemistry* **1988**, *27*, 4305–4310.

(36) Baker, C. H.; Banzon, J.; Bollinger, J. M., Jr.; Stubbe, J.; Samano, V.; Robins, M. J.; Lippert, B.; Jarvi, E.; Resvick, R. *J. Med. Chem.* **1991**, *34*, 1879–1884.

(37) Hoffman, M. Z.; Hayon, E. *J. Am. Chem. Soc.* **1972**, *94*, 7950–7957.

(38) Purdie, J. W.; Gillis, H. A.; Klassen, N. V. *Can. J. Chem.* **1973**, *51*, 3132–3142.

(39) Akhlaq, M. S.; von Sonntag, C. *Z. Naturforsch.* **1987**, *42C*, 134–140.
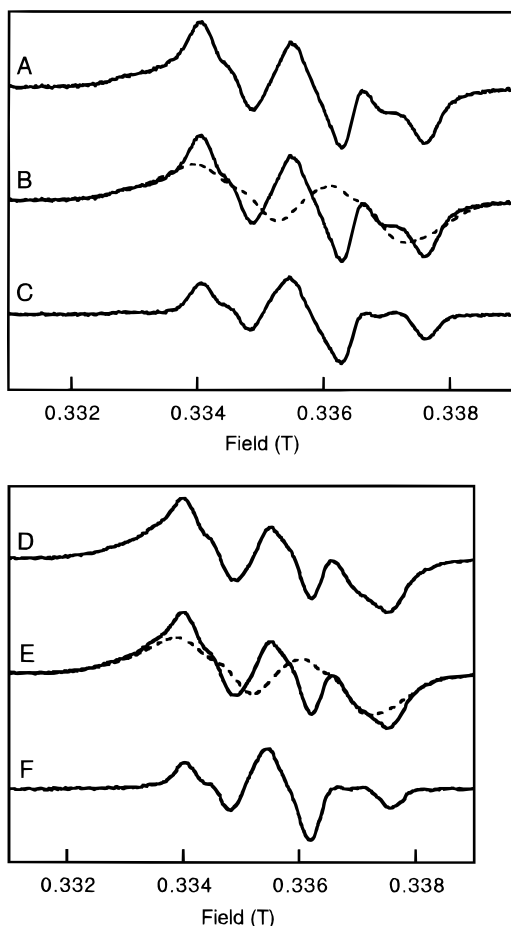
**Figure 1.** (A) EPR spectrum (9.42 GHz) of a sample containing RDPR, (*E*)-**1**, and ATP frozen 1 min after addition of the inhibitor. (B) Superposition of the EPR spectrum of $Y_{122}\cdot$ (- - -) and the spectrum shown in A. The intensity of the Y$^\bullet$ signal was normalized to reflect the radical concentration at $t = 1$ min as quantitated by the absorbance at 410 nm (see the Experimental Section). (C) Spectrum of the new radical intermediate at $t = 1$ min after subtraction of the contribution of the $Y_{122}\cdot$ signal. Spectra D−F are the corresponding spectra for (*Z*)-**1**. Instrument settings for all spectra were as follows: power, 10 $\mu$W; modulation amplitude, 0.39 mT; time constant, 0.126 s; temperature, 101 K.

signal by varying the reaction time, reaction temperature, or concentrations of reactants have been unsuccessful. Therefore, the Y$^\bullet$ line shape, recorded prior to the addition of the inhibitor and appropriately scaled, was subtracted from the experimental spectra to obtain an unobstructed view of the spectrum of the new species (see the Experimental Section for details). This procedure generated very similar line shapes for the paramagnetic species detected in the reactions with either isomer of **1** (Figure 1C,F). While the intensity of these new signals rapidly decayed in solution at 20 °C, the paramagnetic intermediate proved stable for several months in frozen solutions stored at 77 K. The presence or absence of external reductants (DTT or TR/TRR/NADPH) did not have an effect on radical generation, and their appearance was independent of the type of buffer employed (Tris or Hepes).

Spin quantitation was performed on EPR spectra of samples prepared under a variety of conditions. The results showed that the highest ratio of new radical(s) with respect to the total enzyme present was obtained at low protein concentrations and high concentrations of inhibitor. Thus, after 60 s, the reaction of 38 $\mu$M RDPR containing 1.2 equiv of Y$^\bullet$ per enzyme with 750 $\mu$M (*E*)-**1** produced 0.24 equiv of the new radical signal
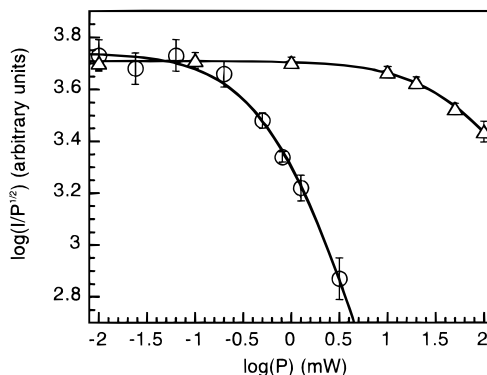


**Figure 2.** Microwave power dependence at 101 K of the integrated intensity of the EPR signals of Y$^\bullet$ (○) and the paramagnetic intermediate (△) formed after a 1-min incubation of RDPR with (*E*)-**1**. Least-squares fits of the data to eq 1 are shown as solid lines. Instrument settings are as in Figure 1.

per equiv of RDPR, while 0.55 equiv of the Y$^\bullet$ signal was lost. This lack of a 1:1 correspondence has been observed under all experimental conditions investigated and is in part due to the instability of the new radical intermediate. Furthermore, the kinetics of tyrosyl radical loss during enzyme inactivation by (*E*)-**1** are multiphasic, suggesting that multiple pathways are responsible for enzyme inactivation.[15] The new radical may only be associated with one of these pathways.

Finally, the variability in the amount of new radical observed is related in part to the protein concentration. The rates of Y$^\bullet$ reduction considerably decreased at protein concentrations of >100 $\mu$M (Y$^\bullet$ loss at 100 $\mu$M is 0.4× that at 38 $\mu$M). While the reason for this observation is unknown, it would be expected to decrease the detectable amount of radical species due to its slower formation.

**Power Saturation Studies of the New Radical.** To probe the relaxation behavior of the new radical, the power dependence of its spectral amplitude was investigated. The data were fit to eq 1,[40,41] in which $I$ is the integrated intensity of the first-

$$\log[I/\sqrt{P}] = \log K - 0.5b \log[1 + (P/P_{1/2})] \qquad (1)$$

derivative (modulation-detected) EPR spectrum, $P$ is the parametrically varied microwave power, $K$ is a sample- and instrument-dependent parameter, $b$ gauges the type of spectral broadening (homogeneous vs inhomogeneous),[42,43] and $P_{1/2}$ is the microwave power at half-saturation of the EPR signal.[44−45] The parameters extracted from fitting the data for the tyrosyl radical in R2 (Figure 2) are $P_{1/2} = 47 \pm 12$ mW and $b = 1.1 \pm 0.2$, values very similar to those reported previously.[45] Its electron spin relaxation rate is considerably enhanced compared to that of a free tyrosyl radical generated by irradiation of a frozen solution, $P_{1/2} = 0.64 \pm 0.19$ mW and $b = 1.48 \pm 0.17$,[44] due to the proximity of the diferric cluster in the protein. Analysis of the power dependence of the new radical spectrum obtained with (*Z*)-**1** provided $P_{1/2} = 0.16 \pm 0.11$ mW and $b = 1.0 \pm 0.17$. Similar results were obtained for the signal generated with (*E*)-**1** (data not shown). The $P_{1/2}$ values for the

(40) Rupp, H.; Rao, K. K.; Hall, D. O.; Cammack, R. *Biochim. Biophys. Acta* **1978**, *537*, 255−269.

(41) Beinert, H., Swartz, H. M., Bolton, J. R., Eds. In *Biological Applications of Electron Spin Resonance*; Wiley-Interscience: New York, 1972; pp 351−410.

(42) Portis, A. M. *Phys. Rev.* **1953**, *91*, 1071.

(43) Castner, T. G., Jr. *Phys. Rev.* **1959**, *115*, 1506.

(44) Chen-Barrett, Y.; Harrison, P. M.; Treffry, A.; Quail, M. A.; Arosio, P.; Santambrogio, P.; Chasteen, N. D. *Biochemistry* **1995**, *34*, 7847−7853.

**Table 1.**[a]



| | simulated radical 5 | | 7[51] | | | | 8[52] | | 9[a] |
| --- | --- | --- | --- | --- | --- | --- | --- | --- | --- |
| | Hα | Hβ | Hα | Hα' | Hβ | Hβ' | Hα | Hα' | Hα' |
| $A_x$, mT | 2.10 | 1.31 | 1.81 | 1.54 | 0.46 | 1.39 | 2.32 | 2.11 | 1.99 |
| $A_y$, mT | 0.70 | 1.41 | 0.60 | 0.51 | 0.46 | 1.39 | 0.76 | 0.68 | 0.64 |
| $A_z$, mT | 1.30 | 1.30 | 1.21 | 1.03 | 0.46 | 1.39 | 1.46 | 1.41 | 1.29 |
| $A_{iso}$, mT | 1.37 | 1.37 | 1.21 | 1.03 | 0.46 | 1.39 | 1.51 | 1.40 | 13.1 |
| $g_1$ | 2.00420 | | 2.0038 | | | | 2.0031 | | 2.0036 |
| $g_2$ | 2.00300 | | 2.0033 | | | | 2.0026 | | 2.0036 |
| $g_3$ | 2.00180 | | 2.0030 | | | | 2.0023 | | 2.0021 |
| $g_{iso}$ | 2.00293 | | 2.0034 | | | | 2.0027 | | 2.0031 |

[a] Heller, C.; Cole, T. *J. Chem. Phys.* **1962**, *37*, 243−250.

new radical and Y• differ by about 2 orders of magnitude. Thus, the power saturation behavior of the new signal suggests that the new paramagnetic species is distant from the diferric cluster.

**Interpretation of 9.4-GHz EPR Spectra.** Docking experiments of the crystal structures of the R1 and R2 subunits of RDPR have suggested that the active site on R1 is ∼35 Å from the diferric cluster−tyrosyl radical cofactor located on R2.[21] Therefore, a substrate-derived radical in the active site of R1 is a possible candidate for the observed paramagnetic intermediate. A fluorinated allyl radical **2,** whose stability is expected to be enhanced by delocalization of the unpaired electron density (Scheme 2), was envisaged to be generated in the first step of the inhibition process. In fact, von Sonntag and co-workers[46] have reported that allylic radicals abstract hydrogen atoms from thiols at much slower rates than nonstabilized alkyl radicals, indicating their decreased reactivity. This suggests that quenching of the radical by one of the cysteines in the active site as proposed in Scheme 2 may be sufficiently slow to allow its detection. Thus, an investigation was undertaken to determine whether the spectra in Figure 1C,F are consistent with assignment of the radical to structure **2**.
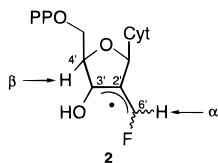


The primary feature of the 9.4-GHz EPR spectra in Figure 1C (or Figure 1F) is a triplet with asymmetric peak intensities and apparent hyperfine interactions on the order of 1.5 mT. This spectrum could arise from electron−nuclear hyperfine coupling to a nucleus with spin 1 (e.g., $^{14}$N) or to two spin-$^1/_2$ nuclei ($^1$H and/or $^{19}$F) whose overlapping doublets could give rise to the observed three-line pattern. The former possibility has been discounted on the basis of spectral simulations that fail to adequately reproduce the experimental spectra (data not shown). Therefore, the possibility of electron−nuclear hyperfine couplings with $^1$H and $^{19}$F nuclei was explored. A survey of the

EPR literature did not reveal data for any monofluorine-substituted allyl radicals. $^{19}$F-hyperfine values of 3.9−7.5 mT have been observed, however, for perfluoroallyl[47] or fluorine substituted α-keto π radicals.[48−50] It thus appears unlikely that a fluorine hyperfine coupling contributes to the spectra in Figure 1. More careful examination of the radical **2** shows a third nucleus that would be expected to give a significant hyperfine interaction to the unpaired electron: the β proton at C-4′. Thus, the spectra in Figure 1C,F cannot be assigned to the fluorinated allyl radical **2**. However, these spectra were optimally simulated using hyperfine parameters that are consistent with values determined previously for a number of nonfluorinated allyl radicals (Table 1). These literature studies have shown that β protons in these species give rise to an isotropic hyperfine coupling of about 1.5 mT, while α protons produce an anisotropic hyperfine coupling with a ratio of 3:1:2 for their principal values (Table 1). For instance, Nelson and co-workers have assigned a radical signal detected during the reaction of lipoxygenase with linoleic acid to the allyl radical **7**.[51] As discussed in more detail below, our best simulations were obtained using one anisotropic and one isotropic hyperfine interaction with values similar to those reported for allyl radicals (Table 1). Thus, one plausible interpretation of the observed spectra (Figure 1) would involve an allyl radical **5** (Table 1) containing one β proton at the 4′ position and one α proton at the 6′ position. In this radical, the fluorine atom would have been replaced by a moiety that would not give rise to any observable hyperfine interaction. The validity of this hypothesis has been tested by isotopic labeling studies as described below.

**The New Radical is Substrate Derived.** In an effort to obtain support for the possible assignment of the observed radical signal to a structure such as **5**, isotope labeling studies were carried out. Previously reported EPR studies[52] suggest that **5** would be expected to have significant spin density on

(45) Sahlin, M.; Petersson, L.; Gräslund, A.; Ehrenberg, A.; Sjöberg, B.-M.; Thelander, L. *Biochemistry* **1987**, *26*, 5541−5548.

(46) von Sonntag, C. In *Free-Radical Reactions Involving Thiols and Disulfides*; Chatgilialoglu, C., Asmus, K.-D., Eds.; Plenum Press: New York, 1990; pp 359−366.

(47) Shedova, M. K.; Allayarov, S. R.; Barkalov, I. M.; Mikhailov, A. I. *Khim. Vys. Energ.* **1987**, *21*, 515−518 (Engl. Transl. 424−426).

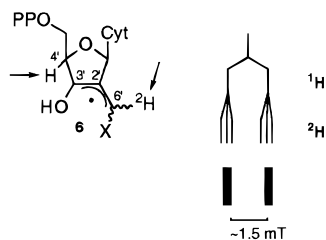(48) Bonazzola, L.; Michaut, J.; Roncin, J. *New J. Chem.* **1990**, *14*, 373−378.

(49) Hasegawa, A.; Wakabayashi, T.; Hayashi, M.; Symons, M. C. R. *J. Chem. Soc., Faraday Trans. 1* **1983**, *79*, 941−951.

(50) Faucitano, A.; Buttafava, A.; Martinotti, F. *Tetrahedron Lett.* **1988**, *29*, 4611−4614.

(51) Nelson, M. J.; Cowling, R. A.; Seitz, S. P. *Biochemistry* **1994**, *33*, 4966−4973.

(52) Maier, G.; Reisenauer, H. P.; Rohde, B.; Dehnicke, K. *Chem. Ber.* **1983**, *116*, 732−740.

**Scheme 3**



C-6′. Thus, substitution of the 6′ proton ($I = \frac{1}{2}$) by a deuterium ($I = 1$) to give **6** (Scheme 3) would be expected to change its EPR spectrum from a pattern of an overlapping doublet of doublets to a pattern of overlapping doublet of triplets. As a result of the substantially smaller gyromagnetic ratio ($\gamma$) of $^2$H compared to $^1$H ($\gamma_D/\gamma_H = 0.15$), the $^2$H triplet splitting would typically be too small to be resolved in our frozen solution spectra. Thus, **6** would be expected to give rise to a doublet signal resulting from hyperfine interaction between the unpaired electron and the proton at the 4′ position as shown in Scheme 3.

To test this prediction, [6′-$^2$H]-(E)-**1** was synthesized by modification of a previously published synthetic route.[53] Incubation of RDPR with [6′-$^2$H]-(E)-**1** for 60 s followed by quenching of the reaction in liquid N$_2$ and analysis of the sample by EPR spectroscopy gave a spectrum that contained both the Y• signal and a signal from additional paramagnetic species. Subtraction of the Y• signal from the resulting spectrum produced the EPR signal shown in Figure 3A. This signal is clearly perturbed from that shown in Figure 1C, suggesting that *the new radical signal is substrate derived*. However, the observed signal is more complex than that predicted (Scheme 3). Overlay of the spectra produced from [6′-$^1$H]-(E)-**1** and [6′-$^2$H]-(E)-**1** offers a possible explanation for this observation (Figure 3B). The low- and high-field edges of the two spectra coincide, suggesting that the triplet signal may actually be present in the spectrum obtained with [6′-$^2$H]-(E)-**1**. Fractional amounts of the triplet signal were then subtracted from the signal in Figure 3B until its features were no longer apparent. This procedure produced the doublet signal shown in Figure 3C, consistent with the prediction in Scheme 3. Spin quantitation established that this doublet and the triplet are present in about equal quantities in Figure 3B. Therefore, this result suggests that the paramagnetic intermediate is substrate derived and that the deuterium at the 6′ position can wash-out to solvent prior to or during its formation.

**Solvent Isotope Studies.** To test the hypothesis that wash-out occurs during RDPR inactivation, (E)-**1** and [6′-$^2$H]-(E)-**1** were incubated with RDPR in $^2$H$_2$O in separate experiments. If the wash-out hypothesis is correct, the new radical signal in the first case would be expected to be a mixture of a doublet and a triplet after subtraction of the Y• signal, while in the second case, the signal associated with the new radical would be expected to be a doublet. The result of the first experiment (Figure 3D) shows a mixture of triplet and doublet signals in a ratio similar to that observed in Figure 3B. The absolute quantity of new signals that were detected under these conditions in several independent experiments was significantly decreased in comparison with reactions performed in H$_2$O, suggesting a solvent isotope effect on the generation and/or decay of the paramagnetic intermediates. This decrease in radical concentration is reflected in the much lower signal-to-noise ratio for the
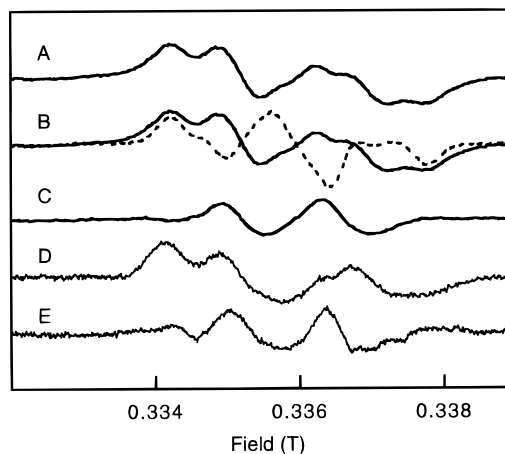
(53) Matthews, D. P.; Persichetti, R. A.; Sabol, J. S.; Stewart, K. T.; McCarthy, J. R. *Nucleosides Nucleotides* **1993**, *12*, 115−123.



**Figure 3.** EPR spectra (9.42 GHz) of the reactions of RDPR with (E)-**1** or (E)-[6′-$^2$H]-**1** under several sets of conditions and following subtraction of the residual Y• spectrum: (A) RDPR and (E)-[6′-$^2$H]-**1** in H$_2$O; (B) RDPR and (E)-**1** in H$_2$O (- - -) overlayed with the spectrum in A (solid line); (C) subtraction of dotted spectrum from solid spectrum in B; (D) RDPR and (E)-**1** in $^2$H$_2$O; (E) RDPR and (E)-[6′-$^2$H]-**1** in $^2$H$_2$O. Instrument settings and incubation times were identical to those in Figure 1.

EPR spectrum in Figure 3D compared to that in Figure 3A. A control experiment was carried out in which [6′-$^2$H]-(E)-**1** was incubated in the absence of enzyme for 24 h under the reaction conditions described above and subsequently analyzed by $^{19}$F NMR (data not shown). The result indicated that $^2$H wash-out requires the presence of RDPR.

Final proof for the existence of a radical species with an associated doublet EPR signal was obtained by incubation of RDPR with [6′-$^2$H]-(E)-**1** in $^2$H$_2$O. As shown in Figure 3E, a doublet signal with width and hyperfine splitting identical to those in Figure 3C was obtained. Once again, only a relatively small amount of the radical (4% of the total protein concentration) was detected in $^2$H$_2$O compared with similar experiments in H$_2$O (up to 25% of the total protein concentration). Despite the lower signal-to-noise ratio of this spectrum, the detection of a doublet in this experiment establishes that the signal obtained with [6′-$^2$H]-(E)-**1** in H$_2$O is composed of a doublet and a triplet. Collectively these solvent isotope studies demonstrate that the 6′-H can wash-out during the inactivation process and that significant spin density resides on or directly adjacent to the 6′ carbon. These results provide strong support that the new radical species is nucleotide based.[54]

**Time Dependence of Fluoride Release.** Efforts to assign the EPR spectra derived from (E)- or (Z)-**1** suggest that fluorine is not present in the radical intermediate. Previous studies on the inactivation of RDPR by 1.5 equiv of (E)-**1** have shown a stoichiometric correlation between the release of fluoride ion and the number of molecules of inhibitor consumed during this process.[15] In these studies, however, fluoride liberation was measured after complete enzyme inactivation. To probe the possibility of replacement of the fluorine on the time scale of the formation of the radical intermediate, the kinetics of fluoride production have been examined using a fluoride electrode

(54) The solvent isotope studies indicate that one of the two hyperfine interactions in the triplet signal originates from the 6′ proton, and the model in Scheme 3 suggests that the second hyperfine interaction would be associated with H4′. To rule out that this second interaction is derived from a proton on R1, uniformly deuterated R1 protein was obtained from *E. coli* grown on $^2$H$_2$O. Incubation of this protein with (E)-**1** and R2 generated an EPR spectrum identical to that shown in Figure 1C (data not shown). This result indicates that both hyperfine couplings in the radical are substrate-derived, consistent with Scheme 3.
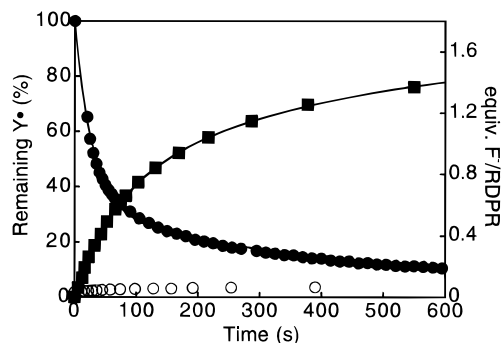
**Figure 4.** Time dependence of fluoride release (■) and loss of the Y•
absorbance at 410 nm (●) during the inactivation of RDPR with (*E*)-
**1**. A control experiment using met-R2 (○) shows that fluoride release
is enzyme-catalyzed. Linear regression fits of the data to double-
exponential equations are indicated by the solid lines through the data
points.

(Figure 4). After 15 min, the reaction of 50 $\mu$M enzyme with
200 $\mu$M (*E*)-**1** produced 1.6 equiv of fluoride per equiv of RDPR
within experimental error of our previous studies.[15] A control
experiment in which R2 was inactivated by reduction of Y• (met-
R2) indicated that this fluoride release is enzyme-dependent
(Figure 4). The data for the time-dependent increase in fluoride
concentration were fit to a double-exponential equation using
nonlinear regression analysis, providing apparent first-order rate
constants of $(1.5 \pm 0.1) \times 10^{-2}$ and $(0.25 \pm 0.03) \times 10^{-2}$ s$^{-1}$.
In a control experiment, it was established that the response
time of the electrode was about 5 times faster than the observed
rate of fluoride release. The EPR spectrum of a sample
withdrawn from the reaction mixture at $t = 35$ s showed that at
this time point 0.06 equiv of new radical was present while
0.34 equiv of fluoride had been released. Therefore, while a
complete time course of radical formation has not been
undertaken, this result suggests that fluoride may be eliminated
prior to formation of the observed radical species.

Finally, the rate of fluoride release has been compared with
the rate of reduction of the tyrosyl radical under identical
conditions (Figure 4). The rate of loss of Y• can be fit to a
double-exponential equation with rate constants of $(3.5 \pm 0.1)
\times 10^{-2}$ and $(0.20 \pm 0.01) \times 10^{-2}$ s$^{-1}$. These results thus
indicate that reduction of Y• occurs faster than release of fluoride
and could be a prerequisite for this process.

**EPR Spectra (139.5 GHz) and Simulations of the New
Radical Species.** There are a large number of parameters
associated with the powder spectra of organic radicals, and
therefore, examination of these species at multiple frequencies
provides an attractive approach to establish their structures. In
particular, high-frequency (95–250 GHz) EPR spectroscopy of
protein-associated free radical species provides a means to
extract additional structural information inaccessible at lower
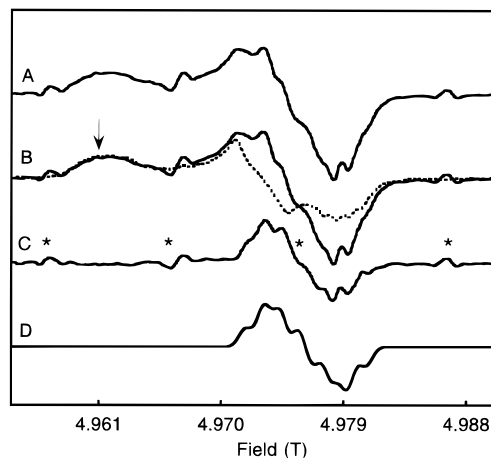frequencies.[25,55-62] EPR spectra (139.5 GHz) obtained upon

(55) Burghaus, O.; Plato, M.; Bumann, D.; Neumann, B.; Lubitz, W.;
Möbius, K. *Chem. Phys. Lett.* **1991**, *185*, 381–386.

(56) Bowman, M. K.; Thurnauer, M. C.; Norris, J. R.; Dikanov, S. A.;
Gulin, V. I.; Tyrshkin, A. M.; Samoilova, R. I.; Tsvetkov, Y. D. *Appl. Magn.
Reson.* **1992**, *3*, 353–368.

(57) Gulin, V. I.; Dikanov, S. A.; Tsvetkov, Y. D.; Evelo, R. G.; Hoff,
A. J. *Pure Appl. Chem.* **1992**, *64*, 903–906.

(58) Gerfen, G. J.; Bellew, B. F.; Un, S.; Bollinger, J. M., Jr.; Stubbe,
J.; Griffin, R. G.; Singel, D. J. *J. Am. Chem. Soc.* **1993**, *115*, 6420–6421.

(59) Prisner, T. F.; McDermott, A. E.; Un, S.; Norris, J. R.; Thurnauer,
M. C.; Griffin, R. G. *Proc. Natl. Acad. Sci. U.S.A.* **1993**, *90*, 9485–9488.

(60) Un, S.; Brunel, L.-C.; Brill, T. M.; Zimmerman, J.-L.; Rutherford,
A. W. *Proc. Natl. Acad. Sci. U.S.A.* **1994**, *91*, 5262–5266.

(61) Un, S.; Atta, M.; Fontecave, M.; Rutherford, A. W. *J. Am. Chem.
Soc.* **1995**, *117*, 10713–10719.



**Figure 5.** (A) EPR spectrum (139.5 GHz) of a sample containing
RDPR, (*E*)-**1**, and ATP in Hepes assay buffer frozen 30 s after addition
of the inhibitor. (B) Superposition of the 139.5-GHz EPR spectrum of
$Y_{122}$• and spectrum A. The spectra were scaled to equalize the spectral
intensity at 4.961 T, which contains exclusively contributions from the
$g_{11}$ tensor of the $Y_{122}$• spectrum. (C) Spectrum of the new radical
obtained by subtraction of the $Y_{122}$• spectrum from A. (D) Simulation
of the new radical spectrum using parameters given in Table 1. All
experimental spectra were obtained as saturated dispersion line shapes
and subsequently pseudomodulated.[25] The asterisks mark peaks arising
from a slight amount of Mn(II) impurity. Experimental conditions are
as follows: temperature, 10 K; modulation amplitude and frequency,
0.2 mT and 400 Hz; time constant, 300 ms; microwave power, 20 $\mu$W.
The simulation (D) was obtained by convolution of the calculated
"stick" spectrum with a saturated dispersion line shape, followed by a
pseudo-modulation procedure identical to that used for the experimental
spectra.

incubation of (*E*)-**1** with RDPR are shown in Figure 5. All
spectra were obtained in the saturated dispersion mode to
maximize signal-to-noise ratios and were subsequently pseudo-
modulated to achieve a conventional "derivative" presentation.[25]
The spectrum of the inhibitor–enzyme mixture contains both
the tyrosyl radical and the new radical species (Figure 5A). The
tyrosyl radical signal was then subtracted from this composite
spectrum to obtain the spectrum of the new radical species
(Figure 5C). Scaling of the tyrosyl radical line shape for these
subtractions was performed by equalizing spectral intensity at
$g = 2.0091$ (4.961 T, Figure 5B). This spectral position, which
is well downfield from the spectrum of the new radical, contains
only intensity from the tyrosyl radical and, thus, provides a
means to calibrate the tyrosyl radical contribution to the reaction
mixture spectrum.[63]

A key component of the analysis of an observed radical
species is the ability to simulate its EPR spectra at different
microwave frequencies using parameters consistent with the
postulated molecular structure. Therefore, simulations of all
the experimentally observed EPR spectra discussed above were
carried out (Figures 5 and 6) as previously described.[25] The
spectra obtained at the magnetic field strengths corresponding
to 139.5-GHz EPR (D-band, 2.14 mm) contain larger contribu-
tions from field-dependent interactions such as the electron
Zeeman interaction. They therefore allow a more accurate
determination of $g$ values than do 9.4-GHz (X-band, 3.2 cm)
spectra. The presence of $g$ anisotropy, not apparent in the low-
frequency spectrum, is readily detected at 139.5 GHz and allows
us to place limits on the $g$ values of the signal derived from the
newly formed radical. The use of these $g$-value constraints in

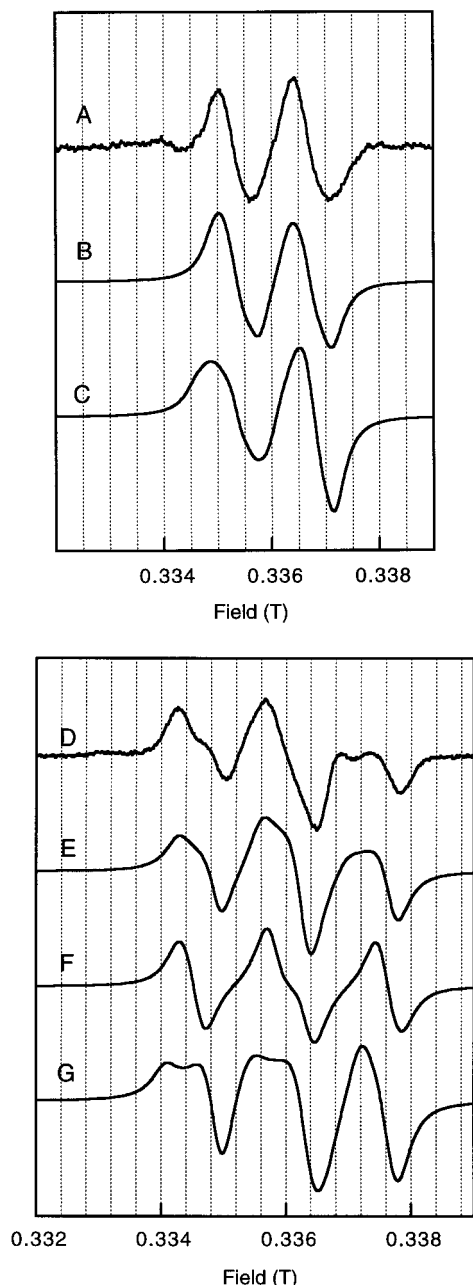(62) Un, S.; Tang, X.-S.; Diner, B. A. *Biochemistry* **1996**, *35*, 679–
684.

**Figure 6.** EPR spectra (9.42 GHz) and simulations of the new radical species. (A) Experimental spectrum obtained in the reaction of RDPR with [6′-²H]-(E)-**1** in D₂O. (B) Simulation of A using the parameters in Table 1, with hyperfine couplings consistent with an α-deuteron (0.3, 0.1, 0.2 mT) and a β proton (1.3, 1.4, and 1.4 mT). The quality of fit parameter (see text) $\chi^2 = 0.013$. (C) Simulation of A using the parameters in Table 1, but with hyperfine couplings consistent with an α deuteron (0.3, 0.1, and 0.2 mT) and an β proton (2.1, 0.7, and 1.3 mT). $\chi^2 = 0.018$. (D) Experimental spectrum obtained in the reaction of RDPR with [6′-¹H]-(E)-**1** in H₂O. (E) Simulation of D using parameters given in Table 1, with hyperfine couplings consistent with one α proton (2.1, 0.7, and 1.3 mT) and one β proton (1.3, 1.4, and 1.4 mT) $\chi^2 = 0.024$. (F) Simulation of D using the same parameters as in E, except for using two essentially isotropic hyperfine couplings (1.8, 1.8, 1.8 mT and 1.3, 1.4, 1.4 mT). $\chi^2 = 0.045$. (G) Simulation of D using the same parameters but with two identical anisotropic hyperfine couplings (2.1, 0.7, and 1.3 mT). $\chi^2 = 0.031$.

the simulation of the spectrum in Figure 3C then yielded the hyperfine coupling values for one spin-$1/2$ species. The most satisfactory simulation of this spectrum was obtained when an isotropic hyperfine interaction was used (Figure 6B). The

hyperfine coupling of the second spin-$1/2$ species was then determined using simulations of both X and D band spectra. The most accurate fits in this case were obtained when substantial anisotropy was introduced into this coupling. Figures 5D and 6E show the spectral simulations at 139.5 and 9.4 GHz, respectively, using the parameter set listed in Table 1, in which the second proton hyperfine coupling displays an anisotropy with a 3:1:2 ratio between the principal values of the *A*-tensor matrix. As mentioned previously, this ratio has also been reported for EPR spectra of other allyl radicals.[52] Use of two isotropic (Figure 6F) or two anisotropic couplings (Figure 6G) produced less adequate simulations regardless of the hyperfine coupling employed. A quantitative estimate of the quality of the fit for the simulations in Figure 6 was obtained by a simplified $\chi^2$ analysis,[64,65] giving the following $\chi^2$ values for the simulations: 0.013 (Figure 6B), 0.018 (Figure 6C), 0.024 (Figure 6E), 0.045 (Figure 6F), and 0.031 (Figure 6G). The presence of a small amount of contaminant Mn(II) in the high-frequency spectrum at 4.976 T (Figure 5C) and imperfect subtraction of the tyrosyl radical at both frequencies may have introduced distortions in the observed spectra and contributed to discrepancies between the simulations and the experimental data. Nevertheless, the simultaneous reproduction of spectra acquired at two EPR frequencies increases the confidence in the spectral fits and, hence, the structural assignment.
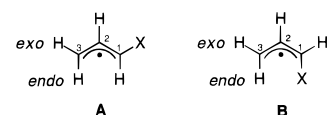
## Discussion

The perturbation of the EPR spectrum produced in the reaction of RDPR with [6′-²H]-(E)-**1** in comparison with (E)-**1** (Figure 3A vs Figure 1C) and the absence of a perturbation of the signal in the reaction with [U-²H]-R1[54] unambiguously establishes that the observed radical intermediate is substrate-derived. Furthermore, these observations also indicate that the radical species carries significant spin density at or adjacent to C6′. This in combination with the *g* values and the size of the hyperfine values of the radical strongly suggests that the observed species represents the first example of a carbon-based radical intermediate produced by RDPR. As discussed in detail below, our previous and current experimental results have led us to propose structure **5** for this nucleotide radical (Table 1). If our assignment is correct, the detection of **5** also provides the first direct support for 3′-hydrogen atom abstraction during the reaction of RDPR with nucleotides.

**Structure of the Paramagnetic Intermediate.** The experimental spectra obtained at 9 and 139.5 GHz of the reaction of RDPR with protonated (E)- or (Z)-**1** in H₂O indicate significant electron−nuclear hyperfine coupling to two nuclear spin-$1/2$ species. One of these couplings persists in the intermediate upon incubation of RDPR with [6′-²H]-(E)-**1** in ²H₂O (Figure 3C). This spectrum could be simulated most accurately using an essentially isotropic hyperfine interaction (Table 1, Figure 6B). These values are consistent with previously reported β-proton hyperfine values in allyl radicals (Table 1, structure **7**[51]). Thus, the experimental data and our spectral simulations are consistent with assignment of this hyperfine coupling to H4′ in **5** (Table 1). Loss of the second hyperfine interaction upon replacement of H6′ with a deuterium provides strong support that this proton constitutes the origin of the second coupling. The most adequate simulations of the experimental data at both 9 and 139.5 GHz were obtained using parameters listed in Table 1, similar to previously reported values for α and β protons in allyl radicals. These results are consistent with structure **5**.

Support for a non-hydrogen substituent X at the 6′ position of the radical species derives from the fact that only one α
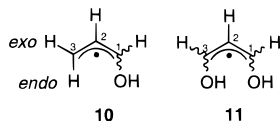
**Table 2**



| conf | X | isotropic hyperfine coupling constant (mT) | | | | ref |
|------|---|-----------------------|--------------------|---------------------|--------------------|-----|
| | | $H_{endo}^{\alpha1}$ | $H_{exo}^{\alpha1}$ | $H_{endo}^{\alpha3}$ | $H_{exo}^{\alpha3}$ | |
| | H | 1.390 | 1.481 | 1.390 | 1.481 | *a* |
| **A** | OH | 1.315 | — | 1.315 | 1.423 | *b* |
| **B** | OH | | 1.386 | 1.333 | 1.386 | *b,c* |
| **A** | OCH$_3$ | 1.305 | — | 1.330 | 1.415 | *d* |
| **B** | OCH$_3$ | | 1.365 | 1.317 | 1.407 | *d* |
| **A** | CO$_{2}$Me | 1.365 | — | 1.280 | 1.365 | *d* |
| **B** | CO$_{2}$Me | | 1.365 | 1.317 | 1.407 | *d* |
| **A** | S$^t$Bu | 1.150 | — | 1.193 | 1.231 | *e* |
| **B** | S$^t$Bu | | 1.17 | 1.250 | 1.190 | *e* |

*a* Kochi, J. K.; Krusic, P. J. *J. Am. Chem. Soc.* **1968**, *90*, 7157. *b* Edge, D. J.; Kochi, J. K. *J. Chem. Soc., Perkin Trans. 2* **1973**, 182−190. *c* Livingston, R.; Zeldes, H. *J. Chem. Phys.* **1966**, *44*, 1245. *d* Sustmann, R.; Trill, H.; Brandes, D. *Chem. Ber.* **1977**, *110*, 245. *e* Griller, D.; Nonhebel, D. C.; Walton, J. C. *J. Chem. Soc., Perkin Trans. 2* **1984**, 1817−1821.

hydrogen is detected in the EPR spectra. The assigned α-proton hyperfine coupling in the observed signal is slightly smaller than that of unsubstituted allyl radicals (Tables 1 and 2), which may indicate a delocalization of spin density from the 6′ carbon onto X and/or onto a substituent elsewhere in the molecule. Table 2 lists the isotropic hyperfine coupling constants of allyl radicals with various substituents in the exo and endo positions. Details of the geometry of the allyl radical **5** (i.e., *E* or *Z*) are unknown at this point, and Table 2 illustrates that the stereochemistry can influence the magnitude of hyperfine couplings. Nonetheless it is instructive to compare the isotropic hyperfine coupling values in Table 2 with the experimentally determined hyperfine coupling for the RDPR-generated radical intermediate. The values of $A_{iso}$ reported for a thioalkyl substituent (1.15−1.24 mT) lie well outside the range determined for the radical species (1.37 ± 0.07 mT), regardless of the radical stereochemistry. Thus, these comparisons suggest that substituent X (Scheme 3) is not a cysteinyl residue. The reported hyperfine values for hydroxy and alkoxy substituents on the other hand lie within the experimental range. Therefore, the most likely candidate for X would be an oxygen-based moiety derived from water or one of the protein residues present in the active site.

Given **5**, the question can be raised as to whether the experimentally determined EPR parameters support the possibility of oxygen substituents at both C3′ and C6′ (X = O). To assess this possibility, given the unavailability of appropriate models, preliminary density functional MO calculations were performed on substituted model allyl radicals **10** and **11**. These



**10**            **11**

calculations predict a reduction in spin density at C1 of ∼6% upon replacement of −H with −OH at C3 (**10** and **11**) regardless of the stereochemistry. Scaling the isotropic hyperfine coupling determined for structure **10**[66] (Table 2) yields an estimate of 1.24−1.30 mT for H1 endo and exo, respectively, in structure **11**. This range is somewhat below the experimental value of 1.37 mT. However, given the uncertainty in radical geometry and the $A_{iso}$ for H$^{\alpha}$ and the simplicity of the model used in the calculation, this analysis suggests that **5** with X = O is feasable.

If X is indeed oxygen-based, the oxygen atom may be derived from water or from a protein residue. Previous studies have indicated that inactivation with [6′-$^{14}$C]-(*E*)-**1** is accompanied by stoichiometric covalent labeling of the R1 subunit.[15] If this covalent adduct and the radical intermediate are associated with the same pathway, then the available X-ray structure of R1 in conjunction with our aforementioned mutagenesis studies suggests that a Glu441 oxygen may be equated with X. Additional support for covalent attachment of the new radical species to a protein residue is presented below in the discussion of the observed deuterium wash-out process.

Our assignment of structure **5** to the observed radical intermediate requires loss of the fluorine substituent prior to formation of the radical. While at present kinetic data for the generation of the radical have not been determined, an upper limit on the rate of its formation is set by the rate of tyrosyl radical reduction. As shown in Figure 4, this rate is about 2-fold faster than the apparent rate of fluoride release with the caveat that the observed rate of fluoride release to bulk solution may be slower than the actual rate of C−F bond cleavage. Since the formation of **5** is most likely several steps removed from reduction of the tyrosyl radical (see below), these data suggest that fluoride release may have occurred prior to the formation of the radical intermediate. Furthermore, the amount of fluoride released exceeds the amount of radical present. Thus, although these results do not prove that fluoride is released prior to the formation of the radical intermediate, the data are consistent with such a postulate. Moreover, the presence of spin density on or adjacent to C6′ as shown by the isotope labeling studies in combination with the absence of a large additional hyperfine interaction expected for an α- or β-fluorine[67] suggests that fluorine has been removed from this position. The 9.4- and 139.5-GHz EPR data and simulations, the power saturation characteristics of the intermediate, the similarity of the EPR parameters with those of previously characterized allyl radicals, the density functional MO calculations, and the kinetics of fluoride release collectively allow us to propose structure **5** for the observed paramagnetic intermediate.

**Proposed Mechanism of Radical Formation.** Our previous hypothesis (Scheme 2) is now expanded to Scheme 4 to generate **5** as suggested by analysis of the EPR data. In this model, an active site residue carries out a Michael addition to **4** and the thiyl radical then abstracts the 6′-hydrogen atom from the Michael adduct **12** to generate **5**.

Several steps in this proposed mechanism (Schemes 2 and

(63) In addition to providing a convenient way to determine the Y• content, the peak corresponding to the principal *g* value = 2.0091 of the Y• spectrum is a sensitive monitor of the molecular and electronic structure of the Y• species. Its spectral position is sensitive to the protonation (or hydrogen-bonding) state of the phenolic oxygen, while the width of the peak is determined by hyperfine splittings to ring ortho and *β* protons and, therefore, sensitive to rotational motion of the aromatic ring. Inspection of Figure 5A,B reveals that the predominant tyrosyl radical species contributing to the *t* = 30 s spectrum is a tyrosyl radical structurally very similar to the tyrosyl radical at *t* = 0 s, since this downfield peak has essentially the same spectral position and width. Thus, the spectral subtraction methodology employed here is valid within experimental uncertainty.

(64) Bevington, P. R. *Data Reduction and Error Analysis for the Physical Sciences*; McGraw-Hill: New York, 1969.

(65) In this analysis, the EPR spectra and simulations were integrated and normalized to unit area. $\chi^2$ was then determined using the following equation, in which $y_i$ and $y'_i$ are the data of the integrated experimental and simulated spectra, respectively:

$$\chi^2 = \sum_i (y_i - y'_i)^2$$

(66) Edge, D. J.; Kochi, J. K. *J. Chem. Soc., Perkin Trans. 2* **1973**, 182−190.

(67) Iwasaki, M. In *Electron Spin Resonance of Irradiated Organic Fluorine Compounds*; Tarrant, P., Ed.; Marcel Dekker: New York, 1971; pp 1−56.

**Scheme 4**



X may represent Glu441
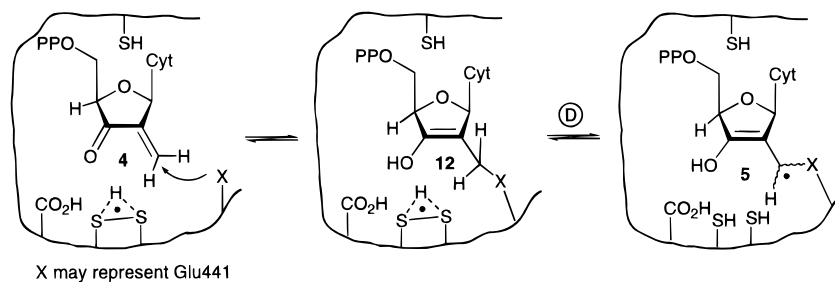
4) require comment. The first is that a thiyl radical can abstract allylic hydrogens (A in Scheme 2, D in Scheme 4). Thermodynamically, this process is feasible since the bond dissociation energies for primary (85.6−89 kcal mol$^{-1}$)[68,69] and secondary allylic C−H bonds (82.5 kcal mol$^{-1}$)[68] are reasonably well matched to those reported for S−H bonds (88.1−91.6 kcal mol$^{-1}$).[68,70,71] At least one example of hydrogen atom abstraction from an allylic position by a thiyl radical has been observed by EPR spectroscopy.[72] The second involves reduction of the relatively unreactive allylic radical[46] **2** (pathway B or C, Scheme 2) by a thiol. However, if the ensuing fluoride elimination from **3,** generated by reduction, is fast, an unfavorable equilibrium in steps B and C could be overcome. Thus the proposed mechanism is feasible on the basis of known chemistry.

The discussion has focused on the reaction of RDPR with (*E*)-**1** as isotopically labeled (*Z*)-**1** is not yet available. However, our hypothesis predicts that the chemistry should be identical with that of (*Z*)-**1**, ultimately leading to the formation of **5**. In fact, the similarity in the 9.4-GHz EPR spectra obtained with (*E*)- and (*Z*)-**1** (Figure 1C,F) suggests that these signals are derived from identical radical intermediates. Preliminary simulations have shown that the EPR signals of allyl radicals that only differ in the geometry of the allyl moiety (*E* vs *Z*) are virtually indistinguishable at 9.4 GHz. Therefore, high-frequency EPR studies on the reaction of RDPR with (*Z*)-**1** and the synthesis of [6′-$^2$H]-(*Z*)-**1** are underway to further test our mechanistic hypothesis (Schemes 2 and 4).

**Proposed Mechanism for Wash-out.** Any proposed mechanism must account for two additional experimental observations. The first is that incubation of RDPR with (*E*)-[6′-$^2$H]-**1** results in wash-out of $^2$H from the observed radical species. The second, and most unusual is that a ∼1:1 mixture of a doublet and triplet species is formed regardless of whether the reactions are carried out in H$_2$O or $^2$H$_2$O, suggesting the absence of a selection effect on the generation of the radical species. The proposed mechanism accounts for both observations. In the case of [6′-$^2$H]-(*E*)-**1**, hydrogen atom transfer from a cysteine to the originally generated deuterium-substituted fluorinated allyl radical will produce the deuterated enol **13** (Scheme 5). Unrestricted rotation around the C2′−C6′ bond of this intermediate would lead to two pathways for fluoride elimination to generate equal quantities of isomeric enones **14** and **15**, in which the deuterium atom occupies either the *E* or *Z* position, respectively. Michael addition of an active site residue would then generate two intermediates in which either a hydrogen or a deuterium atom is juxtaposed to the protonated disulfide

radical.[73] In the former case, hydrogen atom abstraction would generate a deuterated allyl radical which would give rise to a doublet EPR signal. In the latter case, the protonated allyl radical would generate a triplet signal. Thus, the model explains the formation of a mixture of doublet and triplet signals in the inactivation reaction with [6′-$^2$H]-(*E*)-**1**.

This mechanism can also account for the observed stoichiometry of protonated and deuterated radical, ∼1:1. The ratio in which **16** and **17** are formed is expected to be isotope-insensitive, since it is determined only by the face selectivity of fluoride loss. The ratio of **5** to **6** would be solely dependent on the rate constants of their formation in relation to the rate constant for their decay. Kinetic simulation studies have been performed by assuming an intrinsic kinetic isotope effect of 6 on the rate constant for hydrogen/deuterium atom abstraction from **16** or **17** (see the Experimental Section). These studies show that, if the rate of hydrogen atom abstraction from **16** is about 10-fold faster than quenching of the radicals, the ratio of deuterated to protonated radicals would range from 1.05 at $t =$ 30 s to 0.83 at $t =$ 60 s. If the hydrogen atom abstraction is more than 10× faster than the decay rate, this ratio becomes essentially 1:1 at these timepoints. In this case, the relative amounts of the two species only differ significantly at time points 0 s < $t$ < 5 s. Therefore, kinetic studies of the formation and decay of the radical intermediates at early time points using rapid freeze−quench techniques may be mechanistically informative. It must be emphasized that the explanation in Scheme 5 is only valid if the radical intermediate is covalently linked to the protein. If the nucleophilic group X were not derived from a protein active site residue, intermediates **16** and **17** would be expected to have unrestricted rotation around C2′−C6′, resulting in an intramolecular selection against abstraction of a deuterium atom and thereby favoring formation of the deuterated allyl radical at all time points.

Finally, while we favor the mechanistic interpretation in Scheme 4, an alternative mechanism must also be considered (Scheme 6). This model is identical to pathway B in Scheme 2 up to the formation of intermediate **4**, which is in close proximity to a thiyl radical on Cys439. Addition of this radical to the enone would generate the mercapto-substituted α-keto radical **18**.[74] Thiyl radical addition to conjugated unsaturated systems has chemical precedent in the pulse radiolysis literature: thiyl radicals can add to methyl methacrylate to form α-keto radicals.[75] At first glance assignment of the triplet EPR spectrum in Figure 1C to radical **18** may seem unreasonable. This species contains three $\beta$ protons (two at the 6′ and one at the 1′ position) that would be expected to give rise to hyperfine coupling with the unpaired electron. However, the dihedral angle $\theta$ between the p orbital occupied by the unpaired electron

(68) McMillen, D. F.; Golden, D. M. *Annu. Rev. Phys. Chem.* **1982**, *33*, 493−532.
(69) Koppenol, W. H. *FEBS Lett.* **1990**, *264*, 165−167.
(70) Janousek, B. K.; Reed, K. J.; Brauman, J. I. *J. Am. Chem. Soc.* **1980**, *102*, 3125−3129.
(71) Hwang, R. J.; Benson, S. W. *Int. J. Chem. Kinet.* **1979**, *11*, 579.
(72) Lunazzi, L.; Placucci, G. *J. Chem. Soc., Chem. Commun.* **1979**, 533−534.

(73) In Scheme 5, the conjugate addition is arbitrarily drawn to occur from the α face (bottom face) of the enone. Addition from the $\beta$ face would generate the epimers at C6′ of the structures in Scheme 5, but this would still lead to a 1:1 mixture of protonated and deuterated allyl radical species.
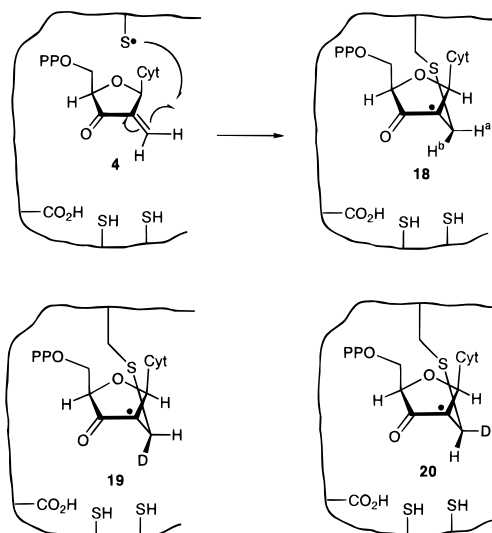
**Scheme 5**



**Scheme 6**
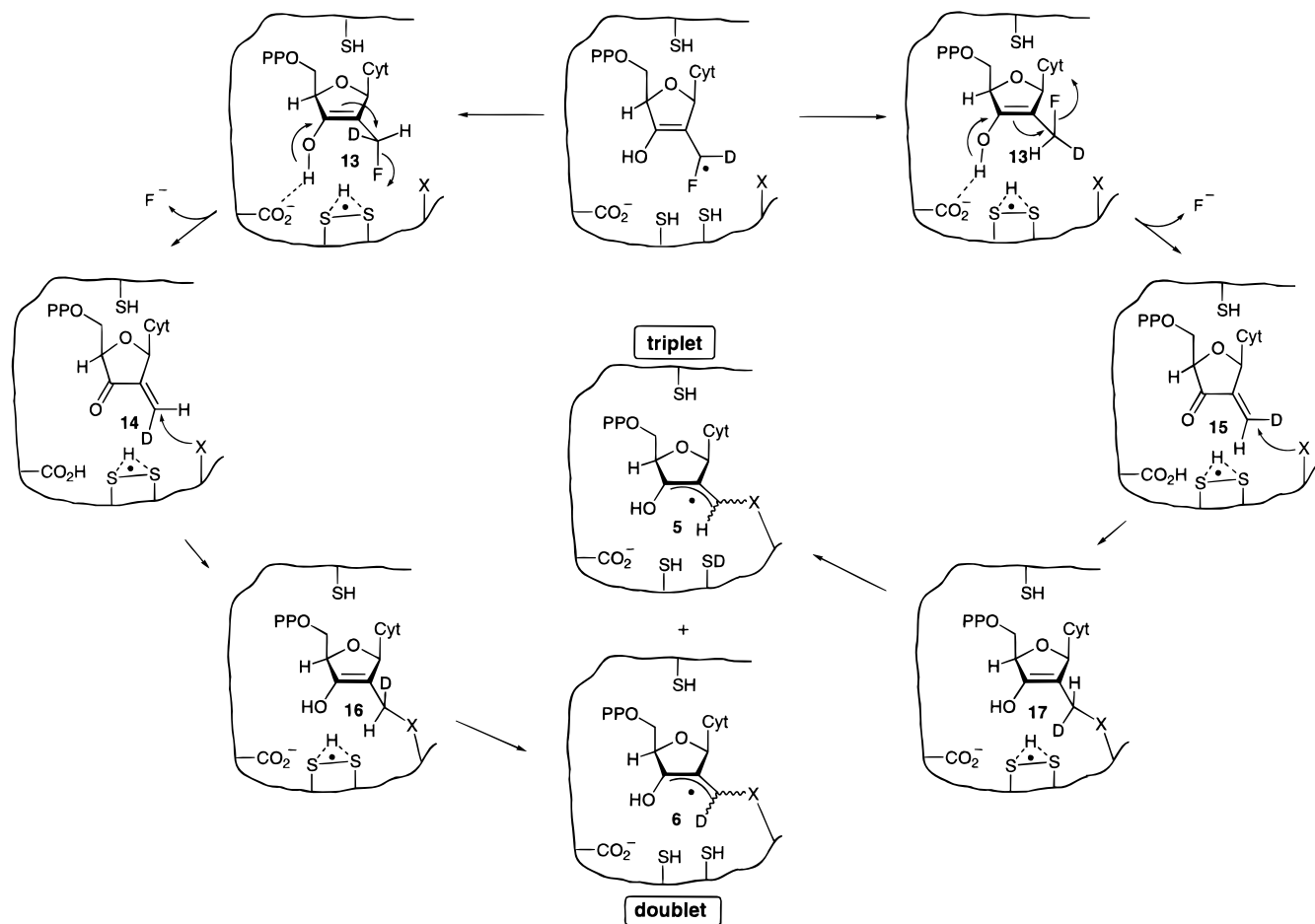


at C2′ and the C–H bond of a $\beta$ proton will determine the size of its hyperfine interaction according to eq 2, in which $\rho_C$ is

$$A_{iso} = \rho_C(C + D \cos^2 \theta + E \cos \theta \cos (\theta + 120)) \quad (2)$$

the spin density on carbon and $C$, $D$, and $E$ are empirically determined constants.[76-81] Constant $C$ is typically on the order of the inhomogeneous EPR line width. Furthermore, if $\theta \approx 90°$ for a C6′ proton (H$^a$) in **18,** then its hyperfine splitting may not be resolved in the EPR spectrum. The two observed hyperfine splittings would then derive from H$^b$ ($\theta \approx 30°$) and from the proton bound to C1′. Thus, in principle, structure **18** could give rise to the spectrum of the new radical species. In addition, the mechanism in Scheme 6 would offer a very straightforward explanation for the observed lack of an isotope effect. When this model is applied to the reaction of RDPR with [6′-$^2$H]-(*E*)-**1** the epimeric radicals **19** and **20** would be formed from intermediates **14** and **15** in about equal amounts.

Using the arguments outlined above, one of these radicals would give rise to a doublet and the other to a triplet. This model therefore requires no isotope effects and no kinetic arguments except that fluoride elimination from **13** (Scheme 5) can occur to the same extent from its $\alpha$ or $\beta$ face. Thus, both the mechanism of radical generation and the explanation of the lack of an isotope effect are very appealing from a chemical perspective.

However, the experimentally determined hyperfine coupling constants for the new radical species and use of eq 2 suggests

(74) Our previous site-directed mutagenesis studies suggest that Cys439 would be the source of the thiyl radical in this model. If the observed radical is associated with the covalent adduct produced when (*E*)-**1** inactivates RDPR, a point not unambiguously established, then of the cysteines in the active site only Cys439 can be involved.[15] Thus, by process of elimination, formation of **18** (Scheme 6) would require that the thiyl radical at Cys439 adds to enone **4** from its $\beta$ face.

(75) Ito, O.; Matsuda, M. *J. Am. Chem. Soc.* **1979**, *101*, 1815.

(76) McConnell, H. M.; Chesnut, D. B. *J. Chem. Phys.* **1958**, *28*, 107.

(77) McLachlan, A. D. *Mol. Phys.* **1958**, *1*, 233.

(78) Heller, C.; McConnell, M. H. *J. Chem. Phys.* **1960**, *32*, 1535–1539.

(79) Wertz, J. E.; Bolton, J. R. *Electron Spin Resonance*; Chapman and Hall: New York, 1986.

(80) Krusic, P. J.; Kochi, J. K. *J. Am. Chem. Soc.* **1971**, *93*, 846–860.

(81) Guerra, M. *Chem. Phys. Lett.* **1987**, *139*, 463.

that structure **18** less readily accommodates available data relative to structure **5**. The values of the constants *C*, *D*, and *E* have been determined previously for β-mercaptoalkyl radicals using molecular orbital calculations.[81] Since, carbonyl groups adjacent to alkyl radical centers can delocalize up to 30% of the spin density, [82] the reported values of $C\rho_C$, $D\rho_C$, and $E\rho_C$ for the mercaptoalkyl radical have been reduced accordingly to give 0.30, 2.67, and 0.23 mT, respectvely.[81] Taking θ values of ∼90 and ∼30 for the two C6′ protons in structure **18** (and assuming typical sp³ hybridization for the −CH₂S fragment giving cos α = cos (θ + 120°)), eq 2 predicts $A_{iso}$ values of ∼0.3 and ∼2.1 mT. The latter value significantly exceeds the experimentally measured hyperfine couplings (1.3−1.4 mT) and is the basis for our tentative dismissal of structure **18** for the RDPR-generated radical intermediate. Since the spin density on the C6′ is expected to differ dramatically between radicals **5** and **18**, EPR studies with [6′-¹³C]-(*E*)-1 will allow a definitive distinction to be made between the mechanisms in Schemes 4 and 6. Synthesis of this compound is currently in progress.

## Conclusion

The EPR studies with an isotopically labeled nucleotide analogue presented here have demonstrated for the first time the presence of a nucleotide-based radical intermediate formed during the inactivation of ribonucleotide reductase by a substrate analogue. Regardless of whether the observed radical is **5** or **18**, these results have strong implications for the mechanism of the normal nucleotide reduction reaction. In both cases the radical can only be produced by abstraction of the 3′-hydrogen atom. Therefore, these studies not only provide the first detection of a substrate-based radical intermediate but also provide additional evidence for abstraction of the 3′-hydrogen atom. These results complement recent reports from this laboratory that have established the importance of thiyl radical chemistry in this class of enzymes[23,25] and provide further support for the proposed mechanism of nucleotide reduction.

## Experimental Section

**Materials.** R1 ($\epsilon_{280\ nm}$ = 189 000 M⁻¹ cm⁻¹), specific activity (SA) 1500∼1700 nmol min⁻¹ mg⁻¹, and R2 ($\epsilon_{280\ nm}$= 130 500 M⁻¹ cm⁻¹, SA 7700∼8000 nmol min⁻¹ mg⁻¹, were prepared as described by Salowe and Stubbe.[83] Prereduced R1 was prepared and characterized as previously described.[18] *E. coli* TR was isolated from SK3981[84] with a SA of 36 units mg⁻¹, and TRR was isolated from K91/pMR14[85] with a SA of 1000 units mg⁻¹. Adenosine 5′-triphosphate (ATP) and reduced β-nicotinamide adenine dinucleotide phosphate (β-NADPH) were obtained from Sigma. DTT was purchased from Mallinckrodt. Hepes assay buffer contained 50 mM Hepes, 15 mM MgSO₄, and 1 mM EDTA (pH 7.6).

**Methods.** UV−vis spectroscopy was carried out using an HP8452A diode array spectrophotometer. EPR spectra at 9.4 GHz were acquired on a Bruker ESP-300 spectrometer at 100 K. Spin quantitation was achieved with a 1.0 mM CuSO₄, 2 M NaClO₄, 0.01 M HCl, 20% (v/v) glycerol standard (*g* = 2.18).[86] Fluoride analyses were determined using an Orion 96−09 fluoride combination electrode. [27]

**Synthesis of [6′-²H]-(*E*)-1.** [6′-²H]-(*E*)-FMC was prepared by a modification of the procedure of Matthews et al.[53] In the last step of the reaction sequence, (*Z*)-2′-[fluoro(tributylstannyl)methylene]-3′,5′-protected cytidine was treated with CsF in MeO²H, providing [6′-²H]-

(*E*)-FMC. The product was judged to be homogeneous by HPLC (Zorbax RxC8, 250 × 4.6 mm column). [6′-²H]-(*E*)-FMC was converted to [6′-²H]-(*E*)-**1** as described previously.[15]

**EPR Studies (9.4 GHz) on the Interaction of (*Z*)- and (*E*)-1 with RDPR.** A spectrum of the Y• was recorded prior to addition of the inhibitor as described in the legend of Figure 1. This sample contained in a final volume of 250 μL: 75 μM prereduced R1, 75 μM R2, 1.6 mM ATP, and 50 mM Hepes assay buffer (pH 7.6). The reaction was initiated by addition of (*E*)-**1** to a final concentration of 300 μM. In addition, reactions carried out in the presence of external reducing equivalents contained 10 mM DTT as reductant or 4.5 μM TR, 0.2 μM TRR and 0.5 mM NADPH. The samples were incubated aerobically at 25 °C for 1 min and then frozen in liquid nitrogen. EPR spectra were recorded with instrument settings described in the legend of Figure 1. To obtain spectra of new paramagnetic intermediates, the signal of Y• was subtracted from the spectra shown in Figure 1A,D. By parametric variation of the fractional amounts of subtracted Y• signal, we constructed difference spectra which were successively better approximations to the new radical signals. Spin quantitation of the amount of Y• subtracted to produce the spectra shown in Figure 1C,F correlated well with the amount of Y• present in the samples just prior to quenching as judged by the drop-line-corrected absorbance at 410 nm.[87] While small changes in the amount of signal subtracted causes differences in the intensities of the remaining features in the difference spectra, their frequencies are much less variable provided that both Y• and the composite signal are recorded under the exact same conditions (see below).

Given the spectral overlap in the radical signals observed (Figure 1), small changes in microwave frequency between recordings of various samples may give rise to artifacts in the signal subtraction procedure described above. The EPR spectrometer used in these experiments was not equipped with a high-accuracy frequency counter. To adjust for any changes in frequency, we employed an internal standard, Mn₀.₀₀₀₂Mg₀.₉₉₉₈O (*g* = 2.001 01 and $A^{Mn}$ = 8.71 mT),[42] located inside a capillary tube, and coinserted with the sample tube into the cavity of the EPR spectrometer. The advantage of this standard is that its sextet resonance lines do not overlap with the signals under investigation. Prior to subtraction, spectra were aligned by superposition of the signals for the manganese standard. The microwave power dependence of the amplitude of signal associated with the new radical species was determined by subtraction of the Y₁₂₂• signal from spectra obtained at various powers.

**EPR Studies (139.5 GHz) on the Interaction of (*E*)-1 with RDPR.** The inactivation mixture contained 125 μM R1, 125 μM R2, 0.9 mM (*E*)-**1**, and 1.6 mM ATP in a final volume of 60 μL of Hepes assay buffer. The reaction was initiated by addition of the inhibitor, and the reaction mixture was incubated at 25 °C for 10 s before being taken up in a fused silica sample tube (i.d. = 0.40 mm, o.d. = 0.55 mm) and frozen in liquid nitrogen at *t* = 30 s. The EPR probe was cooled by immersion in liquid nitrogen, and the sample tube was loaded into the TE₀₁₁ cylindrical resonator of the EPR probe under liquid nitrogen. The probe was then placed inside the Dewar which houses it, which had been previously cooled to a nominal temperature of 80 K; we estimate the temperature of the sample never exceeded 10 K.
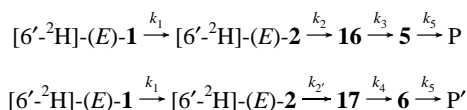
**Time-Dependent Release of Fluoride and Reduction of Y•.** The release of fluoride during the inactivation of RDPR by (*E*)-**1** was monitored using a fluoride electrode inserted into the reaction vessel. The sample contained in a final volume of 1 mL: 50 μM prereduced R1, 50 μM R2, 1.6 mM ATP, and 50 mM Hepes assay buffer (pH 7.6). TR, TRR, and NADPH were omitted from the assay since they were found to interfere with the electrode readings (data not shown). An aliquot of a stock NaF solution was then added to the assay solution to a final concentration of 75 μM. This provided a constant initial electrode reading and ensured that the fluoride concentrations measured were within the linear portion of a standard curve generated under identical conditions. In a control experiment, it was verified that this addition of fluoride did not affect the enzyme activity nor its inactivation by **1**. The inhibition reaction was initiated by addition of (*E*)-**1** to a

(82) Camaioni, D. M.; Walter, H. F.; Jordan, J. E.; Pratt, D. W. *J. Am. Chem. Soc.* **1973**, *95*, 7978−7992.

(83) Salowe, S. P.; Stubbe, J. *J. Bacteriol.* **1986**, *165*, 363−366.

(84) Lunn, C. A.; Kathju, S.; Wallace, B. J.; Kushner, S.; Pigiet, V. *J. Biol. Chem.* **1984**, *259*, 10469−10474.

(85) Russell, M.; Model, P. *J. Bacteriol.* **1985**, *163*, 238−242.

(86) Malmström, B.; Reinhammar, B.; Vänngård, T. *Biochim. Biophys. Acta* **1970**, *205*, 48.

(87) Bollinger, J. M., Jr.; Edmonson, D. E.; Huynh, B. H.; Filley, J.; Norton, J. R.; Stubbe, J. *Science* **1991**, *253*, 292−298.

final concentration of 200 $\mu$M. The time-dependent change in electrode potential was recorded.

Two control experiments were carried out. First it was verified that the release of fluoride was enzyme-dependent by performing the reaction with R2 that had been inactivated by reduction of Y$^{\bullet}$ with 15 mM hydroxyurea for 20 min. Second, the dead time of the electrode response was determined under the conditions of the assay described above. Aliquots of NaF stock solution were added to a solution of the same composition as described above, and the electrode reading was followed as a function of time. The response could be fitted to a first-order process with a rate constant of 0.09 $\pm$ 0.02 s$^{-1}$. The time dependence of the reduction of Y$^{\bullet}$ was examined in a parallel experiment under identical conditions by monitoring its characteristic absorbance at 410 nm as previously reported.[87]

**Kinetic Simulations.** The simulations of the ratio of protonated to deuterated radicals was performed with HopKINSIM 1.7.2 software using the following kinetic schemes:

$$[6'-{}^2\text{H}]-(E)\text{-}\mathbf{1} \xrightarrow{k_1} [6'-{}^2\text{H}]-(E)\text{-}\mathbf{2} \xrightarrow{k_2} \mathbf{16} \xrightarrow{k_3} \mathbf{5} \xrightarrow{k_5} \text{P}$$

$$[6'-{}^2\text{H}]-(E)\text{-}\mathbf{1} \xrightarrow{k_1} [6'-{}^2\text{H}]-(E)\text{-}\mathbf{2} \xrightarrow{k_{2'}} \mathbf{17} \xrightarrow{k_4} \mathbf{6} \xrightarrow{k_5} \text{P}'$$

In these schemes, P and P$'$ represent the products of quenching of the radicals **5** and **6** and $k_2$ represents the net rate constant for three chemical reactions which transform **2** into **16** or **17**. As a first approximation the observed rate of reduction of Y$^{\bullet}$ was taken for $k_1$. The values of $k_2$, $k_3$, and $k_5$ were then varied to account for about 0.15 equiv of **16** formed at $t = 60$ s. Then, $k_4$ was set to $k_3/6$ to provide an intrinsic isotope effect of 6 and the ratio of $k_3/k_5$ was varied from 1.0 to 1000. The program then calculated the rate profiles for the formation of **5** and **6** and their ratio from $t = 0$ to $t = 60$ s.

**Density Functional Calculations.** Theoretical calculations were performed with the GAUSSIAN94 (Revision D.3) suite of programs[88]

on an IBM RS6000. Slater's local spin density exchange function[89] and the local spin density correlation functional of Vosko, Wilk, and Nusair[90] (SVWN) were employed with the 6-31G(d)[91,92] basis set. The SVWN/6-31G(d) basis set has previously been found to give good agreement with experimental spin densities, vibrational frequencies, and structures for the neutral and cation indolyl radicals[93]—models for tryptophan—as well as the neutral phenoxy and tyrosyl radicals[94] and the tyrosyl cation radical.[95] The geometries of the unsubstituted and all the oxygen- and sulfur-substituted allyl radicals were optimized at the SVWN/6-31G(d) basis set level. An optimized C–O bond length of 1.35 Å was obtained for both singly and doubly substituted oxygen allyl radicals. An optimized C–S bond length of 1.73 Å was obtained for the sulfur-substituted allyl radical. The expectation value of $\langle S^2 \rangle$ $= S(S + 1) = 0.75$ for all calculations indicates that the calculated ground states are good representations of the doublet state of the $S = {}^1\!/_2$ radical.

Wong, M. W.; Andres, J. L.; Replogle, E. S.; Gomperts, R.; Martin, R. L.; Fox, D. J.; Binkley, J. S.; Defrees, D. J.; Baker, J.; Stewart, J. P.; Head-Gordon, M.; Gonzalez, C.; Pople, J. A. *Gaussian 94, Revision D.3*; Gaussian, Inc.: Pittsburgh, PA, 1994.

(89) Slater, J. C. *Quantum Theory of Molecules and Solids*; McGraw-Hill: New York, 1974; Vol. 4.

(90) Vosko, S. H.; Wilk, L.; Nusair, M. *Can. J. Phys.* **1980**, *58*, 1200–1211.

(91) Hehre, W. J.; Radom, L.; Schleyer, P. V. R.; Pople, J. A. *Ab Initio Molecular Orbital Theory*; Wiley: New York., 1986.

(92) Davidson, E. R.; Feller, D. *Chem. Rev.* **1986**, *86*, 681–696.

(93) Walden, S. E.; Wheeler, R. A. *J. Phys. Chem.* **1996**, *100*, 1530–1535.

(94) Qin, Y.; Wheeler, R. A. *J. Am. Chem. Soc.* **1995**, *117*, 6083–6092.

(95) Qin, Y.; Wheeler, R. A. *J. Phys. Chem.* **1996**, *100*, 10554–10563.

(88) Frisch, M. J.; Trucks, G. W.; Schlegel, H. B.; Gill, P. M. W.; Johnson, B. G.; Robb, M. A.; Cheeseman, J. R.; Keith, T.; Petersson, G. A.; Montgomery, J. A.; Raghavachari, K.; Al-Laham, M. A.; Zakrzewski, V. G.; Ortiz, J. V.; Foresman, J. B.; Peng, C. Y.; Ayala, P. Y.; Chen, W.;